Photochemistry of Butyrophenone: Combined Complete-Active-Space Self-Consistent Field and Density Functional Theory Study of Norrish Type I and II Reactions

Hong-Yuan He and Wei-Hai Fang*

Department of Chemistry, Beijing Normal University, Beijing 100875, People's Republic of China

David Lee Phillips*

Department of Chemistry, The University of Hong Kong, Pokfulam Road, Hong Kong S.A.R., People's Republic of China

Received: December 6, 2003; In Final Form: April 16, 2004

The complete-active-space self-consistent field (CASSCF) and density functional theory (DFT) approaches have been used to study the mechanistic details of Norrish type I and II reactions of aromatic carbonyl compounds, with butyrophenone ($PhCOCH_2CH_2CH_3$) as a representative. A minimum energy crossing point was found to exist among three potential energy surfaces (S_1, T_1, and T_2), and the three-surface crossing allows the T_2 state to act as a relay that enables the intersystem crossing (ISC) from S_1 to T_1 to occur with a high efficiency for $PhCOCH_2CH_2CH_3$. Once the molecule is in the T_1 state, the 1,5-H shift reaction is the predominant reaction pathway and yields a triplet 1,4-biradical of $PhC(OH)CH_2CH_2CH_2$ as an intermediate species. Since the formation of excited triplet products is energetically improbable, the subsequent decomposition, cyclicization, and disproportionation of the 1,4-biradical proceed after intersystem crossing from the triplet to singlet state. The singlet 1,4-biradical was found to have three isomers, which determine to a certain extent the branching ratios of the subsequent reactions. The study given here provides new insights into the S_1 relaxation dynamics of aromatic carbonyl compounds and their subsequent reaction mechanisms.

Introduction

Photoexcitation ($n \rightarrow \pi^*$) of a ketone from the ground state (S_0) to its first excited singlet state (S_1) may lead to breakage of the α bond (Norrish type I reaction).[1−4] When a ketone contains γ C−H bonds, the 1,5-hydrogen shift reaction (Norrish type II reaction) can also take place,[5−14] forming a 1,4-biradical. There are three competing pathways following the primary hydrogen abstraction. The first pathway is the cyclization of the biradical to give the cyclobutanol product (Norrish−Yang cyclization). The second pathway is the cleavage of the C−C single bond to give an enol and the corresponding alkene products (Norrish II cleavage). The third pathway is the hydrogen back-transfer to reconstitute the starting material in its electronic ground state. The mechanistic details and the related dynamics of these Norrish type I and II reactions are essential to understanding the photochemistry of ketones and related carbonyl compounds.

The photochemistry of aliphatic ketones has been the subject of numerous studies over many decades. A classic example is the photodissociation of acetone, which has been reviewed by Zewail and co-workers in recent work.[1−4] A general picture for the observed S_1 dynamics of acetone and related aliphatic ketones (R′COR, where R′ and R = methyl, ethyl, isopropyl, and *tert*-butyl) has been determined in previous studies.[1,2,5,6,10] Upon $n \rightarrow \pi^*$ excitation, the molecules in the S_1 state can overcome the barrier on the S_1 surface down to the S_1/S_0 conical region, where the molecules go back to the ground state, leading to either α cleavage radical pairs or hot parent molecules. The molecules in the S_1 state can also undergo intersystem crossing from the S_1 Franck−Condon region to the T_1 state, followed by α C−C cleavage along the T_1 pathway to form radical pairs. Whether the α C−C bond cleavage proceeds along the singlet or triplet n,π^* pathway for aliphatic ketones is dependent on the excitation wavelength.[1,2,5,6,10] These experimental conclusions were supported by recent theoretical studies.[1,2,13,15−17]

The conjugation interaction between the aromatic ring and the carbonyl group has a noticeable influence on the relative energies of the $n\pi^*$ and $\pi\pi^*$ states as well as their chemical reactivity. Therefore, the relaxation dynamics and dissociation mechanisms for the excited aromatic carbonyl molecules are different from those for the corresponding aliphatic carbonyl compounds. Numerous experimental studies[18−31] have been done to explore laser photoexcitation spectra, properties of the intramolecular excited charge-transfer states, hydrogen abstraction from hydrogen-donating compounds, structural differences between the $n\pi^*$ and $\pi\pi^*$ triplet states, excited-state lifetimes, and photoinduced reactions for benzaldehyde, acetophenone, butyrophenone, and valerophenone. Experimentally, it has been well established that aromatic carbonyl compounds have certain similarities. First, the S_1 state lifetime for aromatic ketones (ArCOR) was found to be much shorter than that for aliphatic ketones in the gas and condensed phases. Second, aromatic carbonyl compounds are highly phosphorescent but only weakly fluorescent molecules. Third, both singlet and triplet $n\pi^*$ states can undergo type I and II Norrish reactions for aliphatic ketones, but both reactions occur from the lowest triplet state for most aromatic ketones or aldehydes.

Although some rules of thumb were obtained for Norrish type I and II reactions of aromatic ketones on the basis of numerous

* Corresponding authors: (W.-H.F.) fax (+86)-10-6220-5382, e-mail fangwh@bnu.edu.cn; (D.L.P.) fax (+852)-2857-1586, e-mail phillips@hkucc.hku.hk.

10.1021/jp037735l CCC: $27.50
Published on Web 05/28/2004

experimental observations,[14] ab initio calculations have been done mainly for aliphatic carbonyl compounds.[32−37] To our knowledge, there are only two reports[38,39] that involve ab initio studies on the mechanistic photochemistry of aromatic carbonyl compounds. We recently observed that several aromatic carbonyl compounds have a triple potential energy crossing point between the S_1, T_1, and T_2 states; this was reported in a short communication.[38] Experimentally, it has been found that butyrophenone bearing a leaving group on the α carbon can produce benzoylcyclopropane with a reasonable yield upon $n \rightarrow \pi^*$ excitation.[40] We have explored this new cyclopropanation pathway from a theoretical perspective.[39]

Here we report a systematic theoretical examination of Norrish I and II reactions of butyrophenone ($PhCOCH_2CH_2CH_3$) upon $n \rightarrow \pi^*$ excitation, which serves as a representative of aromatic ketone containing a γ C−H bond. The S_1, T_1, and T_2 potential energy surfaces were found to intersect in the Franck−Condon region, which gives a reasonable explanation for why the intersystem crossing (ISC) to the T_1 state is so efficient in isolated molecules of aromatic ketones. A minimum-energy crossing point between the two lowest singlet-state surfaces (S_1/S_0) was determined, which is similar to the 1,4-biradical in structure. The singlet/singlet internal conversion and the triplet/singlet intersystem crossing were found to play an important role in the subsequent cyclization, elimination, and disproportionation of the 1,4-biradical. We believe that the results reported here provide new insights into the interesting and complex photochemistry of aromatic carbonyl compounds.

Computational Methods

The complete-active-space self-consistent field (CASSCF) wave function has sufficient flexibility to model the changes in electronic structure upon electronic excitation.[41] In conjunction with a proper basis set, the CASSCF method can provide a balanced description of the minimum-energy structures on the S_0, T_1, S_1, T_2, and S_2 states of $PhCOCH_2CH_2CH_3$. It is also worth mentioning that the CASSCF method is appropriate in this case because the relative differential dynamic correlation of the excited states with respect to the ground state is fairly constant. In principle, all of the valence electrons and orbitals of a system should be included in the active space for the CASSCF optimizations. In practice, this is not feasible for the systems investigated here, because of our limited computational capability. Thus, the selection of the active space becomes a crucial step for the CASSCF calculation. The active space is composed of 10 electrons distributed in nine orbitals, hereafter referred to as CAS(10,9). From the viewpoint of the localized picture of the molecular orbitals, the active space is composed of the three π and three π^* orbitals in the aromatic ring, the C−O π and π^* orbitals, and the oxygen nonbonding orbital. The state-averaged (SA) CASSCF method[42] was used to determine geometry on the intersection space of two different electronic states. One π^* orbital with an occupation very close to 0.0 was not included in the active space for the SA-CASSCF optimizations.

The equilibrium geometries and transition-state structures on the S_0 and T_1 surfaces have been optimized by the B3LYP method. The B3LYP method has been demonstrated to be computationally efficient and can give a satisfactory reproduction of the observed structures, barrier heights, and transition energies.[43,44] The nature of the critical points (equilibrium geometries and transition states) was confirmed by an analytical frequency computation at the B3LYP level of theory. Geometry optimizations were carried out to the standard convergence

CHART 1

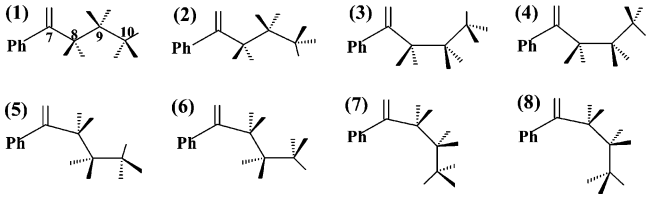

CHART 2

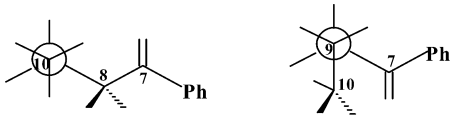

criteria: a maximum element of the gradient of less than 0.000 45 hartree/bohr (0.54 kcal mol^{-1} $Å^{-1}$) and a RMS of gradient element of less than 0.0003 hartree/bohr (0.36 kcal mol^{-1} $Å^{-1}$). The 6-31G, 6-31G*, and 6-311G** basis sets were used to optimize the structures and to calculate the energies. A factor of 0.98 was used to scale the B3LYP calculated zero-point energies in the calculation of barrier heights and the dissociation energies.[45] The CASSCF and DFT calculations were performed with the Gaussian 98 package of programs.[46]

Results and Discussion

Structures and Relative Energies of the Low-Lying Electronic States. The conformational situation at the ground-state level can be correlated with its photochemical behavior if the reactions proceed directly on short-lived excited states. As shown in Chart 1, eight possible conformations exist for $PhCOCH_2CH_2CH_3$ under a constraint of C_s symmetry. However, the B3LYP/6-311G** calculations predict that only conformation **1** is an energy minimum in the ground state. Conformations **2**, **4**, and **6** have been confirmed to be the first-order saddle points governing rotations of the terminal CH_3 group around the C9−C10 single bond, of the CH_2−CH_3 group around the C8−C9 single bond, and of the CH_2−CH_2−CH_3 group around the C7−C8 single bond, respectively. The other conformations are the second-, third-, or fourth-order saddle points. With respect to structure **1**, the saddle points **2**, **4**, and **6** have energy of 2.8, 7.9, and 6.9 kcal/mol, respectively. The structure of $PhCOCH_2CH_2CH_3$ in the ground state was reoptimized without any symmetry constraint. A nonplanar minimum was found from the B3LYP/6-311G** optimization that is energetically equal to structure **1**. As shown schematically in Chart 2, the nonplanar minimum has an anti conformation with respect to the C8−C9 and C9−C10 single bonds.

The T_1 equilibrium geometry was found to be nonplanar for $PhCOCH_2CH_2CH_3$. With respect to the T_1 equilibrium geometry, the C_s-symmetric T_1 structure has a relative energy of 0.9 kcal/mol at the UB3LYP/6-311G** level of theory. The C_s-symmetric S_0, S_1, T_1, S_2, and T_2 structures for $PhCOCH_2CH_2CH_3$, which correspond to the ground, $^1n\pi^*$, $^3n\pi^*$, $^1\pi\pi^*$, and $^3\pi\pi^*$ states, were optimized at the CAS(10,8) and CAS(10,9) levels of theory with the 6-31G and 6-31G* basis sets. The resulting structures and energies are given in the Supporting Information. The CAS(10,9)/6-31G* structures for $PhCOCH_2CH_2CH_3$ in the S_0, S_1, T_1, S_2, and T_2 states are depicted in Figure 1 with the atom-labeling scheme illustrated in the S_0 structure. In the ground state, the aromatic ring is almost a regular hexagon with the C−C−C angle in the range of 119.8−120.3° and the largest difference of 0.012 Å in the C−C bond length. With respect to the S_0 structure, the most striking change in the T_1

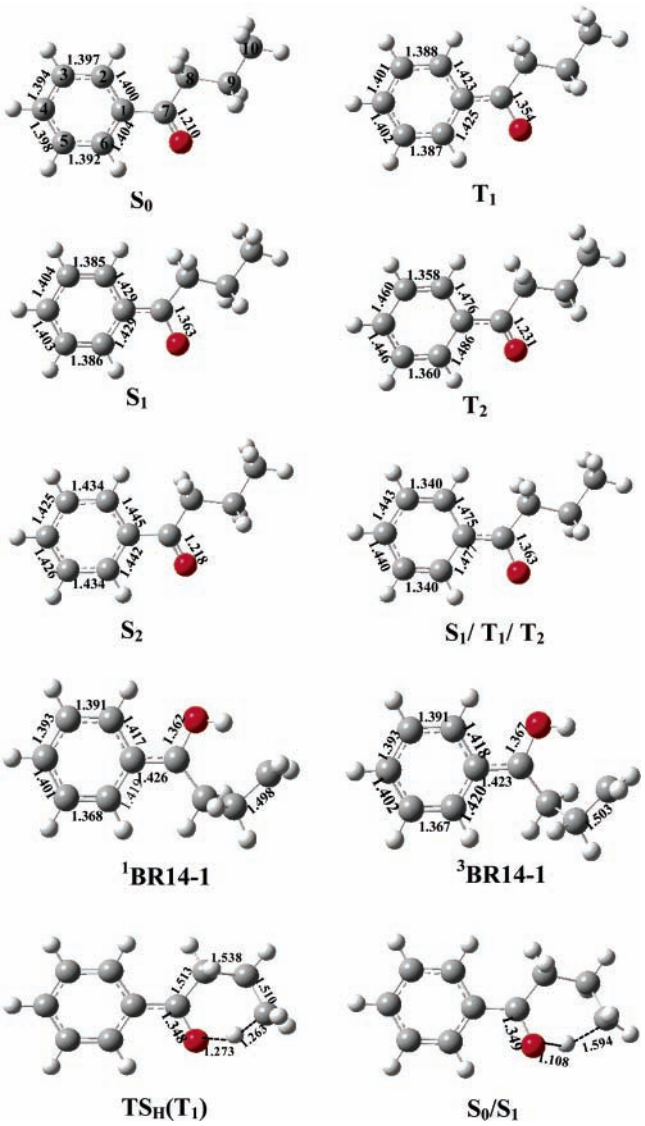

Figure 1. Schematic structures for the selected stationary and intersection points, along with the key bond parameters (bond lengths in angstroms, bond angles in degrees) and the atom-labeling scheme illustrated in the S_0 structure.

CHART 3

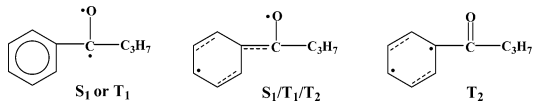

or S_1 structure is associated with the C−O bond length. As shown in Figure 1, the C−O bond length is 1.210 Å in the ground state, and it becomes 1.354 and 1.363 Å in the T_1 and S_1 structures, respectively. The $n \rightarrow \pi^*$ transition of carbonyl compounds is dominated by progressing in the C═O stretching mode that reflects substantial change in the C−O bond length. It is reasonable to expect that the $n \rightarrow \pi^*$ transition only has a little influence on the structure of the aromatic ring.

The S_1 and T_1 electronic states are of similar biradical character, which is described in Chart 3. However, there is a large difference in the S_2 and T_2 structures. In the T_2 state, the C2−C3 and C5−C6 bond distances are about 1.36 Å, and the two bonds are mainly of double-bond character. The other C−C bond distances in the aromatic ring are close to the C−C single-bond length. Natural orbital analysis shows that two singly occupied π orbitals are mainly composed of the $2p_z$ orbitals of C1 and C4 atoms (the $x-y$ plane is the symmetric plane). The CAS(10,9)/6-31G* structure and molecular orbitals clearly reveal that the T_2 state is a biradical with the two unpaired electrons in the C1 and C4 atoms and two double bonds in the C2−C3 and C5−C6 regions. The structural features of the T_2 state are shown in Chart 3. In the S_2 state, two unpaired electrons are delocalized into the whole aromatic ring, which results in an uniform increase of the ring C−C bonds from ~1.40 Å in S_0 to ~1.43 Å in S_2. The $\pi \rightarrow \pi^*$ transition is mainly localized in the aromatic ring. One can expect that this transition has a large influence on structures of the aromatic ring, but the carbonyl group is less influenced by the $\pi \rightarrow \pi^*$ transition.

The adiabatic excitation energies to T_1, S_1, T_2, and S_2 were calculated to be 75.9, 78.8, 75.5, and 105.9 kcal/mol, respectively, at the CAS(10,9)/6-31G* level of theory. In comparison with the corresponding experimental 0−0 energy values of 72.0 (25 183 cm^{-1}), 76.9 (26 919 cm^{-1}),[47] 76.1 (3.3 eV),[48] and 100.6 (35 191 cm^{-1})[19] kcal/mol for PhCHO and 73.7 (25 791 cm^{-1}),[48] 77.9 (27 279 cm^{-1}),[47] and 101.2 kcal/mol (35 402 cm^{-1})[49] to the T_1, S_1, and S_2 states of $PhCOCH_3$, respectively, the present computations give a reasonably good estimation of the relative energies for the low-lying electronic states of $PhCOCH_2CH_2CH_3$. The π and σ orbitals are well separated in energy for the aromatic carbonyl compounds that contain relatively large π conjugation systems. The near-degenerate orbitals are included in the (10,9) active space of the CASSCF calculations given here, and this is one of the reasons why the relative energies predicted by the CAS(10,9) calculations are close to the experimental values.

$S_1/T_2/T_1$ Three-Surface Intersection. To investigate the S_1 relaxation dynamics, we searched for the minimum energy crossing points between the singlet- and triplet-state surfaces and the crossing points between the two triplet surfaces, respectively. The detailed structures and energies for the intersections are available in the Supporting Information. The singlet and triplet surface crossing was determined by use of Slater determinants in the state-averaged CASSCF calculations and was identified as the $S_1(^1n\pi^*)$ and T_2 ($^3\pi\pi^*$) surface crossing (S_1/T_2). Similarly, the intersection between the two triplet surfaces was identified as one between the T_2 and T_1-($^3n\pi^*$) surfaces (T_2/T_1). The optimized structures show that S_1/T_2 and T_2/T_1 are indistinguishable from one another in structure and the two crossing points have the same energy. In fact, the S_1, T_1, and T_2 surfaces intersect in the same region ($S_1/T_2/T_1$) for $PhCOCH_2CH_2CH_3$. The geometric and electronic structures of the $S_1/T_2/T_1$ intersection are described in Figure 1 and Chart 3. An analogous three-surface intersection was found for PhCHO and $PhCOCH_3$.[38] It has been found that the structure of the PhCO moiety is very similar in the $S_1/T_2/T_1$ intersections for all of the aromatic carbonyl compounds investigated so far. The $S_1/T_2/T_1$ three-surface intersection has been reported for acrolein[33] and this molecular system can serve as a useful prototype or model for PhCOR molecular systems. The $S_1/T_2/T_1$ surface intersection is likely a common feature for many aromatic carbonyl compounds with a nearly constant structure.

In the S_1 or T_1 structure, two unpaired electrons are populated mainly in the carbonyl C and O atoms, while the two singly occupied electrons are mainly in the aromatic ring in the T_2 structure. As shown in Chart 3, the $S_1/T_2/T_1$ structure is located between $S_1(T_1)$ and T_2 with the two unpaired electrons distributed in the O atom and the aromatic ring, respectively. The differences in the S_1 and $S_1/T_2/T_1$ structures mainly result from the redistribution of the conjugation π electrons and thus would not be expected to give rise to a substantial change in

the energy. The $S_1/T_2/T_1$ structure is 6.9 and 85 kcal/mol above the S_1 and S_0 minima, respectively. The $S_0 \rightarrow S_1$ absorption of ArCOR has a large predominant progression in the C−O stretching mode with a broad peak centered at ∼325 nm[22] and the corresponding vertical excitation energy is about 90 kcal/mol. After photoexcitation, the relaxation from the S_1 Franck−Condon (FC) geometry to the $S_1/T_2/T_1$ region only involves deformation of the conjugation PhCO moiety and this takes place easily. In view of the structures and the energies found here for the FC point, the S_1 and the $S_1/T_2/T_1$ intersection, the initially excited wave packet starts from the FC geometry on the S_1 surface and can readily travel to reach the $S_1/T_2/T_1$ intersection.

As discussed in our recent communication,[38] direct $S_1(^1n\pi^*) \rightarrow T_1(^3n\pi^*)$ intersystem crossing for PhCOR would be expected to occur with a low efficiency or rate because there is no first-order spin−orbit coupling for the $S_1 \rightarrow T_1$ transition. However, the $S_1(^1n\pi^*) \rightarrow T_2(^3n\pi^*)$ ISC process happens with high efficiency due to a strong spin−orbit interaction.[50] The T_2/T_1 crossing point is a conical intersection between the T_2 and T_1 surfaces, and the time scale for the $T_2 \rightarrow T_1$ internal conversion (IC) process via the conical intersection may be expected to be on the order of a vibrational period.[51] Therefore, the existence of the $S_1/T_2/T_1$ intersection results in the $S_1 \rightarrow T_1$ process to take place via the T_2 state. The T_2 state functions as a relay and enables the $S_1 \rightarrow T_1$ ISC to take place with a high rate. It has been well-established experimentally that the magnitude of intersystem crossing rates (k_{ST}) are about 10^{11} s^{-1} for aromatic ketones,[50,52−56] while the k_{ST} values for aliphatic ketones are in the range of $10^{7-}10^8$ s^{-1}.[57,58] The existence of the $S_1/T_2/T_1$ intersection can help explain the 1000-fold difference in the ISC rates between aromatic and aliphatic ketones.

Norrish Type I Reactions. The α C−C bond cleavage may occur along the S_1 reaction pathway. The fragments of PhCO-(X^2A') and $CH_2CH_2CH_3(X^2A)$ are nondegenerate in the ground state. When the two fragments approach each other, they can correlate adiabatically with $PhCOCH_2CH_2CH_3$ in the ground and triplet states. Qualitatively, the α C−C bond cleavage along the S_1 pathway gives rise to fragments of $PhCO(A^2A'') + CH_2$-$CH_2CH_3(X^2A)$ in an excited electronic state, which is different from the α C−C bond cleavage along the T_1 pathway that leads to fragments in the ground state. This qualitative analysis predicts that the α C−C bond cleavage for $PhCOCH_2CH_2CH_3$ has a high barrier on the S_1 pathway. The S_1 transition state was optimized at the CAS(10,8) level of theory with the 6-31G* basis set. The barrier height to the S_1 PhCO−$CH_2CH_2CH_3$ bond cleavage was estimated to be about 35 kcal/mol at the CAS-(10,8)/6-31G* level of theory. As pointed out before, the $S_1/T_2/T_1$ intersection is only 6.9 kcal/mol above the S_1 minimum, and the T_2 state functions as a relay and enables the $S_1 \rightarrow T_1$ ISC to take place with a high rate. Therefore, the α C−C bond cleavage along the S_1 pathway is not in competition with the S_1 relaxation to the T_1 state via the $S_1/T_2/T_1$ intersection.

The $PhCOCH_2CH_2CH_3$ molecules in the T_1 state can dissociate into PhCO + $CH_2CH_2CH_3$ and Ph + $COCH_2CH_2CH_3$ along the T_1 pathways. Transition states for the two reactions were determined from the UB3LYP/6-311G** optimizations [labeled TS1(T_1) and TS2(T_1), respectively]. The C−C distances are 2.144 and 2.204 Å in TS1(T_1) and TS2(T_1), respectively. The α C−C bond cleavages are accompanied by a decrease in the C−O bond length in order to form the ground-state radical of $COCH_2CH_2CH_3$ or PhCO with the Ph or $CH_2CH_2CH_3$ radical as a coproduct. The α PhCO−$CH_2CH_2CH_3$ bond cleavage has a barrier height of 18.0 kcal/mol, while the barrier height for the α Ph-$COCH_2CH_2CH_3$ bond cleavage is 28.3 kcal/mol.

It is well-known that $n \rightarrow \pi^*$ excitation results in a pyramidal T_1 equilibrium structure for aliphatic carbonyl compounds such as H_2CO, CH_3CHO, and CH_3COCH_3. This is due to the C═O π bond being weakened by the excitation and the $^3n\pi^*$ state becoming sp^3-hybridized at the carbonyl C atom. However, the aromatic ring and the C═O moiety are actually coplanar in the T_1 equilibrium geometry for aromatic carbonyl compounds and this primarily results from the conjugation interaction between the aromatic ring and the C═O moiety that stabilizes these types of molecules. The conjugation interaction between the aromatic ring and the carbonyl group makes the Ph−$COCH_2CH_2CH_3$ bond stronger than the PhCO−$CH_2CH_2CH_3$ bond, and this is the main reason that a relatively low barrier exists on the T_1 pathway of PhCO−$CH_2CH_2CH_3$ bond cleavage. The dissociation reaction of $PhCOCH_2CH_2CH_3 \rightarrow PhCO + CH_2CH_2CH_3$ is endothermic by 6.2 kcal/mol, while the $PhCOCH_2CH_2CH_3$ decomposition into Ph + $COCH_2CH_2CH_3$ is endothermic by 21.4 kcal/mol. The relatively high endothermicity for the latter reaction is another reason that a relatively high barrier exists on the $PhCOCH_2CH_2CH_3$ decomposition into Ph + $COCH_2$-CH_2CH_3 reaction pathway.

With respect to the S_0 minimum, the barrier height of the T_1 PhCO−$CH_2CH_2CH_3$ bond fission is 85.4 kcal/mol for $PhCOCH_2$-CH_2CH_3. Electronic excitation to the S_1 state of $PhCOCH_2CH_2$-CH_3 gives rise to the ∼320 nm absorption band manifold with a vertical excitation energy of about 90 kcal/mol. It is evident that the PhCO−$CH_2CH_2CH_3$ bond cleavage reaction along the T_1 pathway is accessible with ∼320 nm excitation. Kinetic analysis suggested a triplet-state rate constant of $\sim 10^5$ s^{-1} for the α-cleavage reaction of substituted $PhCOCH_2CH_2CH_3$ in different solvents.[29,31] In comparison with the experimental rate of reaction, the barrier (18.0 kcal/mol) for the α-cleavage reaction of $PhCOCH_2CH_2CH_3$ appears somewhat overestimated by our present UB3LYP/6-311G** calculations.

The 1,5-H Shift Reactions. Once the $PhCOCH_2CH_2CH_3$ molecules relax to the T_1 surface, the 1,5-H shift can take place. The stationary structures on the T_1 potential energy surface for the 1,5-H shift reaction have been optimized by the DFT method at the UB3LYP/6-311G** level of theory. The transition state for the 1,5-H shift, referred to as $TS_H(T_1)$ in Figures 1 and 2, was obtained and confirmed to be the first-order saddle point on the T_1 potential energy surface. Rotation and deformation of the terminal CH_2CH_3 group takes place prior to the H atom transfer. As shown in Figure 2, the 1,5-H shift reaction has a barrier of 6.2 kcal/mol. This barrier is much lower than that of 18.0 kcal/mol found on the α C−C bond cleavage pathway. The 1,5-H shift reaction is the predominant pathway from the T_1 state of $PhCOCH_2CH_2CH_3$. In comparison with the experimental rate constant[29,30] of $(8 \times 10^6)\sim(1 \times 10^8)$ s^{-1}, the calculated barrier of 6.2 kcal/mol is reasonable for the T_1 1,5-H shift reaction.

The triplet lifetime of valerophenone in water was estimated to be about 7 times longer than that observed in hydrocarbon solvents.[30] Since the triplet lifetime is controlled by the 1,5-H shift reaction, these results indicate that the rate constant for the 1,5-H shift reaction is significantly lowered in aqueous media. The CAS(10,9)/6-31G* calculations predict that the planar $^3n\pi^*$ and $^3\pi\pi^*$ states of $PhCOCH_2CH_2CH_3$ are nearly equal in energy. However, a large difference exists in the dipole moment of the two triplet states. The dipole moments are 1.49 D for the $^3n\pi^*$ state and 2.81 D for the $^3\pi\pi^*$ state at the CAS-(10,9)/6-31G* level of theory. The $^3\pi\pi^*$ state is stabilized more

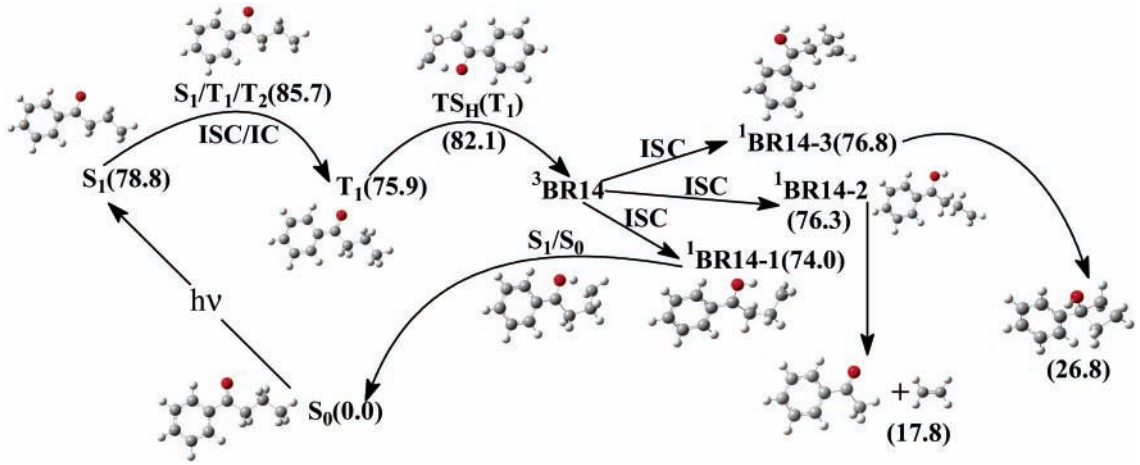

Figure 2. Detailed processes for the Norrish type II reaction of butyrophenone and schematic structures of the stationary and intersection points on the reaction pathways. The relative energies (kilocalories per mole) are given in parentheses.

than the $^3n\pi^*$ state when the solvent is changed from a nonpolar organic medium to water. This greater stabilization of the $^3\pi\pi^*$ state in a polar solvent is likely mainly responsible for the longer lifetimes observed for aromatic alkyl ketones in aqueous media compared to their lifetimes in nonpolar organic solvents. Solvent-induced changes in the relative levels of reactive $^3n\pi^*$ and unreactive $^3\pi\pi^*$ states of aromatic alkyl ketones are known to affect their triplet reactivities.[5]

Structure of the 1,4-Biradical. As shown in Figure 2, there are three competing pathways following the 1,5-H shift reaction that leads to formation of a 1,4-biradical of $PhC(OH)CH_2CH_2$-CH_2. The 1,4-biradical can decompose into $PhC(OH)CH_2$ + CH_2CH_2 (Norrish II cleavage), undergo a cyclization reaction (Norrish−Yang cyclization) to form the cyclobutanol product, and disproportionate back to the ground-state ketone. Three minimum-energy structures were found for the biradical in the lowest triplet state, which are labeled ^{3}BR14-1, ^{3}BR14-2, and ^{3}BR14-3, respectively. The ^{3}BR14-1 structure is the most stable with relative energies of 0.8 and 1.4 kcal/mol for ^{3}BR14-2 and ^{3}BR14-3, respectively, at the UB3LYP/6-311G** level of theory. The isomerization processes among the three isomers involve only a rotation of the CH_2 or CH_2CH_2 group around the C−C single bond, and the barrier was estimated to be 2−4 kcal/mol by the UB3LYP/6-311G** calculations.

Three structures for the singlet 1,4-biradical were determined by the CAS(10,8)/6-31G* optimizations, which are respectively labeled ^{1}BR14-1, ^{1}BR14-2, and ^{1}BR14-3 in Figure 2. ^{1}BR14-1 is the most stable with relative energies of 2.3 and 2.8 kcal/mol for ^{1}BR14-2 and ^{1}BR14-3, respectively. For comparison, the ^{3}BR14-1, ^{3}BR14-2, and ^{3}BR14-3 structures were reoptimized at the CAS(10,8)/6-31G* level. The resulting bond lengths and angles for the triplet 1,4-biradical are very close to those for the corresponding singlet 1,4-biradical. ^{1}BR14-1, ^{1}BR14-2, and ^{1}BR14-3 are 0.8, 0.1, and 0.5 kcal/mol lower than ^{3}BR14-1, ^{3}BR14-2, and ^{3}BR14-3, respectively. By use of Slater determinants in the state-averaged CAS(10,8)/6-31G* calculations, the intersection points between the triplet and singlet surfaces were determined for the 1,4-biradical. There is no change in structure from the triplet 1,4-biradical to the corresponding intersection point, except for a small deformation of the $CH_2CH_2CH_2$ moiety of the biradical. The triplet/singlet intersection point and the triplet and singlet 1,4-biradicals are very close to each other in energy. If the triplet/singlet intersystem crossing can be treated as a spin-allowed process, the time scale for the process is expected to be on the order of a rotational period ($\sim 10^{-11}$ s) of the CH_3 group around the C−C single bond.

Norrish II Cleavage, Norrish−Yang Cyclization, and Disproportionation Reactions. With respect to the ^{3}BR14-2 zero-level point, the UB3LYP/6-311G** calculations obtain a barrier of 26.9 kcal/mol for the decomposition reaction along the triplet pathway. The calculated barrier height reveals that the triplet-state decomposition into $PhC(OH)CH_2$ + CH_2CH_2 is very difficult for the 1,4-biradical. If the Norrish−Yang cyclization proceeds along the spin-conservation T_1 pathway, the cyclobutanol derivative is formed in its excited triplet electronic state. The T_1 cyclization process requires a large amount of energy to overcome the high endothermicity of this reaction and probably occurs with little probability. The lifetime of about 10^{-7} s found for the triplet 1,4-biradical in solution[6,59,60] eliminates any reasonable possibility that a major reaction pathway for the triplet biradical has a large barrier or high endothermicity.

Since the spin-conservation triplet state reactions take place with less probability for the triplet 1,4-biradical, intersystem crossing from the triplet to the singlet state plays a predominant role in the subsequent reactions. In conjunction with the state-averaged CAS(10,8)/6-31G* wave functions, a one-electron spin−orbit Hamiltonian with effective nuclear charges was used to calculate the spin−orbit coupling (SOC) matrix elements between the triplet and the singlet 1,4-biradicals. The calculated SOC values are respectively 0.4, 0.2, and 0.2 cm^{-1} for the ^{3}-BR14-1, ^{3}BR14-2, and ^{3}BR14-3 structures. On the basis of the calculated SOC value and the differences of the energy gradients at the intersection point region, the probability factor (a transition probability per passage through the crossing seam) from the triplet to singlet state is estimated to be 5×10^{-4} by the Landau−Zener law.[61] The rate of the triplet−singlet ISC is reduced by a factor of about 5×10^{-4}, as compared with that ($\sim 10^{11}$ s^{-1}) for the spin-allowed process. This is consistent with the lifetime of about 10^{-7} s found for the triplet 1,4-biradical in the solution phase.

It can be seen from the structures of the three isomers (Figure 2) that ^{1}BR14-2 gives exclusively cleavage products, while ^{1}-BR14-1 and ^{1}BR14-3 are favorable conformers for disproportionation to the ground state and Norrish−Yang cyclization, respectively. No barrier exists on the singlet Norrish−Yang cyclization pathway, and this predicts that cyclization proceeds very fast. However, there are some other factors that should also be considered and these can significantly reduce the rate of cyclization. The singlet biradical is sp^2-hybridized at the C atom bonded to the aromatic ring, whereas the cyclobutanol to be formed is sp^3-hybridized at this carbon atom. A large

deformation takes place for the formation of the cyclobutanol and this requires some additional energy. The entropy value decreases by ~9.0 cal mol^{-1} K^{-1} in the cyclization process, which reduces the rate constant significantly for this reaction. Although these factors hinder the formation of the cyclobutanol product, the singlet 1,4-biradical of ^{1}BR14-3 can undergo cyclization with reasonably high efficiency.

The singlet 1,4-biradical can decompose into $PhC(OH)CH_2 + CH_2{=}CH_2$ along the singlet pathway. A transition state was found on the decomposition pathway of ^{1}BR14-2. With respect to the zero level of ^{1}BR14-2, the barrier to the decomposition was estimated to be 11.5 kcal/mol by the CAS(10,8)/6-31G* calculations and the singlet 1,4-biradical decomposition to $PhC(OH)CH_2 + CH_2{=}CH_2$ is predicted to take place easily along the singlet pathway. Once the singlet $PhC(OH)CH_2$ radical is formed, it isomerizes very easily to $PhCOCH_3$ in the ground state.

Disproportionation is an important pathway for the triplet 1,4-biradical to deactivate, and this includes intersystem crossing to the singlet state and reverse hydrogen transfer to the ground-state ketone. The disproportionation process involves a change in the nature of the electronic state from an open-shell singlet 1,4-biradical to a closed-shell ground-state ketone. A minimum-energy crossing point between the open-shell and closed-shell singlet state surfaces (S_1/S_0) was found by a state-averaged CAS-(10,8)/6-31G optimization. The S_1/S_0 conical intersection is similar to the 1,4-biradical in structure. The disproportionation of the singlet 1,4-biradical takes place very easily through the S_1/S_0 conical intersection to the ground-state ketone. As noted before, ^{3}BR14-1 is the most stable among the three triplet isomers and a similar situation occurs for ^{1}BR14-1. The SOC value for ^{3}BR14-1 is larger than that for BR14-T/S-2 or BR14-T/S-3. It is reasonable to expect that ^{1}BR14-1 is produced with a relatively large probability. As a result, more than 50% of the 1,4-biradical disproportionates to the ground-state ketone. Experimentally, it has been found that 40% of the 1,4-biradical intermediate was converted into the $PhCOCH_3 + CH_2{=}CH_2$ and cyclobutanol products with a decomposition/cyclization ratio of about 1/2 for butyrophenone.[31] This is consistent with our present computational results.

Summary

The CASSCF and DFT approaches have been used to study the mechanistic details of the Norrish type I and II reactions for a representative aromatic carbonyl compound: butyrophenone ($PhCOCH_2CH_2CH_3$). It was found theoretically that a minimum energy crossing point exists among the three potential energy surfaces (S_1, T_1, and T_2) and this appears to be common to a wide variety of aromatic carbonyl compounds with a constant structure. Since there is no first-order spin−orbit coupling for the $S_1 \rightarrow T_1$ transition, the direct $S_1(^1n\pi^*) \rightarrow T_1(^3n\pi^*)$ intersystem crossing for $PhCOCH_2CH_2CH_3$ takes place with low efficiency. The existence of the $S_1/T_2/T_1$ intersection leads the $S_1 \rightarrow T_1$ process to occur via the T_2 state where the T_2 state functions as a relay and allows the S_1 to T_1 ISC to take place with a high rate of reaction or efficiency. This appears to be one of the main reasons why the intersystem crossing (ISC) from S_1 to T_1 is very efficient for aromatic carbonyl compounds and both the α-cleavage and hydrogen abstraction reactions occur from the lowest triplet state for most aromatic ketones.

Once the $PhCOCH_2CH_2CH_3$ molecules are in the lowest triplet state, the α-C−C bond cleavage can take place, but the 1,5-H shift is the predominant channel that yields the triplet 1,4-biradical as an intermediate. Since the formation of excited triplet products is energetically improbable, the subsequent cyclization, decomposition, and disproportionation reactions proceed from the singlet 1,4-biradical. On the basis of the optimized structures, the calculated energies and SOC values, the triplet−singlet ISC process is predicted to occur with a rate of about 10^7 s^{-1} and this value is consistent with the lifetime of about 10^{-7} s found for the triplet 1,4-biradical in the solution phase. The singlet 1,4-biradical was found to have three isomers, ^{1}BR14-1, ^{1}BR14-2, and ^{1}BR14-3, that determine to a certain extent the branch ratios of the subsequent reactions. ^{1}BR14-2 gives exclusively cleavage products, while ^{1}BR14-1 and ^{1}BR14-3 are favorable conformers for the disproportionation to the ground state and the Norrish−Yang cyclization reactions, respectively. The detailed mechanism for the Norrish type II reactions of butyrophenone is summarized in Figure 2.

Acknowledgment. This work was supported by grants from the National Natural Science Foundation of China (Grant 20233020) and from the Ministry of Science and Technology of China (Grant 2002CB613406) to W.H.F. and by a grant from the Research Grants Council of Hong Kong (HKU 7108/02P) to D.L.P.

Supporting Information Available: Optimized structures and energies for the stationary and intersection points reported in this study. This information is available free of charge via the Internet at http://pubs.acs.org.

References and Notes

(1) Diau, E. W.-G.; Kotting, C.; Zewail, A. H. *ChemPhysChem* **2001**, *2*, 273−293.
(2) Diau, E. W.-G.; Kotting, C.; Zewail, A. H. *ChemPhysChem* **2001**, *2*, 294−309.
(3) Diau, E. W.-G.; Kotting, C.; Solling, T. I.; Zewail, A. H. *ChemPhysChem* **2001**, *3*, 57−78, and references therein.
(4) Diau, E. W.-G.; Kotting, C.; Solling, T. I.; Zewail, A. H. *ChemPhysChem* **2001**, *3*, 79−97 and references therein.
(5) Wagner, P. J. *Acc. Chem. Res*. **1971**, *4*, 168−177 and references therein.
(6) Scaiano, J. C. *Acc. Chem. Res*. **1982**, *15*, 252−258 and references therein.
(7) Wagner, P. J. *Acc. Chem. Res*. **1989**, *22*, 83−90 and references therein.
(8) Horspool, W.; Armesto, D. *Organic Photochemistry: A Comprehensive Treatment*; Ellis Harwood Limited: Chichester, U.K., 1992; p 195.
(9) Gilbert, A.; Baggott, J. *Essentials of Molecular Photochemistry*; CRC Press: Boca Raton, FL, 1991; p 310.
(10) Wagner, P. J. In *CRC Handbook of Organic Photochemistry and Photobiology*; Horspool, W. M., Song, P.-S., Eds.; CRC Press: Boca Raton, FL, 1995; p 449.
(11) Feyter, S. D.; Diau, E. W.-G.; Zewail, A. H. *Angew. Chem., Int. Ed*. **2000**, *39*, 260−263.
(12) Reddy, G. D.; Jayasree, B.; Ramamurthy, V. *J. Org. Chem*. **1987**, *52*, 3107−3113.
(13) Liu, D.; Fang, W.-H.; Fu, X. Y. *Chem. Phys. Lett*. **2000**, *325*, 86−92.
(14) Griesbeck, A. G.; Heckroth, H. *J. Am. Chem. Soc*. **2002**, *124*, 396−403.
(15) Setokuchi, O.; Simizu, Y. *J. Mol. Struct. (THEOCHEM)* **1997**, *401*, 29−33.
(16) Setokuchi, O.; Matuzawa, S.; Simizu, Y. *Chem. Phys. Lett*. **1998**, *284*, 19−23.
(17) Sakurai, H.; Kato, S. *J. Mol. Struct. (THEOCHEM)* **1999**, *461*, 145−152.
(18) Molina, V.; Merchan, M. *J. Phys. Chem A*. **2001**, *105*, 3745−3751 and references therein.
(19) Silva, C. R.; Reilly, J. P. *J. Phys. Chem*. **1996**, *100*, 17111−17123 and references therein.
(20) Berger, M.; Goldblatt, I. L.; Steel, C. *J. Am. Chem. Soc*. **1973**, *95*, 1717−1725.
(21) Berger, M.; Steel, C. *J. Am. Chem. Soc*. **1975**, *97*, 4817−4821.
(22) Zhao, H.-O.; Cheung, Y.-S.; Liao, C.-L.; Liao, C.-X.; Ng, C. Y. *J. Chem. Phys*. **1997**, *107*, 7230−7241.
(23) Warren, J. A.; Bernstein, E. R. *J. Chem. Phys*. **1986**, *85*, 2365−2367.

(24) Kapturkiewicz, A.; Nowacki, J. *J. Phys. Chem. A* **1999**, *103*, 8145−8155.
(25) Matsushita, Y.; Yamaguchi, Y.; Hikida, T. *Chem. Phys.* **1996**, *213*, 413−419.
(26) Srivastava, S.; Yourd, E.; Toscano, J. P. *J. Am. Chem. Soc.* **1998**, *120*, 6173−6174.
(27) Baronavski, A. P.; Owrutsky, J. C. *Chem. Phys. Lett.* **2001**, *333*, 36−40.
(28) Osterheld, T. H.; Brauman, J. I. *J. Am. Chem. Soc.* **1990**, *112*, 2014−2016 and references therein.
(29) Lewis, F. D.; Hilliard, T. A. *J. Am. Chem. Soc.* **1972**, *94*, 3852−3858.
(30) Zepp, R. G.; Gumz, M. M.; Miller, W. L. *J. Phys. Chem. A* **1998**, *102*, 5716−5723 and references therein.
(31) Wagner, P. J.; McGrath, J. M. *J. Am. Chem. Soc.* **1972**, *94*, 3849−3851.
(32) King, R. A.; Allen, W. D.; Schaefer, H. F., III *J. Chem. Phys.* **2000**, *112*, 5585−5592.
(33) Fang, W.-H. *J. Am. Chem. Soc.* **1999**, *121*, 8376−8384.
(34) Fang, W.-H. *J. Am. Chem. Soc.* **2000**, *122*, 10886−10894.
(35) Chen, X.-B.; Fang, W.-H. *J. Am. Chem. Soc.* **2003**, *125*, 9689−9698.
(36) Yamamoto, N.; Olivucci, M.; Celani, P.; Bernardi, F.; Robb, M. A. *J. Am. Chem. Soc.* **1998**, *120*, 2391−2407.
(37) Wilsey, S.; Gonzalez, L.; Robb, M. A.; Houk, K. N. *J. Am. Chem. Soc.* **2000**, *122*, 5866−5876.
(38) Fang, W.-H.; Phillips, D. L. *ChemPhysChem.* **2002**, *3*, 889−892 (communication).
(39) Fang, W.-H.; Phillips, D. L. *J. Theor. Comput. Chem.* **2003**, *2*, 23−31.
(40) Wessig, P.; Muhling, O. *Angew. Chem., Int. Ed.* **2001**, *40*, 1064−1065.
(41) Schmidt, M. W.; Gordon, M. S. *Annu. Rev. Phys. Chem.* **1998**, *49*, 233−266.
(42) (a) Frisch, M. J.; Ragazos, I. N.; Robb, M. A.; Schlegel, H. B. *Chem. Phys. Lett.* **1992**, *189*, 524−528. (b) Yamamoto, N.; Vreven, T.; Robb, M. A.; Frisch, M. J.; Schlegel, H. B. *Chem. Phys. Lett.* **1996**, *250*, 373−378.
(43) Wiberg, K. B.; Stratmann, R. E.; Frisch, M. J. *Chem. Phys. Lett.* **1998**, *297*, 60−70.
(44) Chen, W.-C.; Yu, C.-C. *J. Chem. Phys.* **2001**, *115*, 7495−7502 and references therein.
(45) Scott, A. D.; Radom, L. *J. Phys. Chem.* **1996**, *100*, 16502−16513.
(46) Frisch, M. J.; Trucks, G. W.; Schlegel, H. B.; Scuseria, G. E.; Robb, M. A.; Cheeseman, J. R.; Zakrzewski, V. G.; Montgomery, J. A., Jr.; Stratmann, R. E.; Burant, J. C.; Dapprich, S.; Millam, J. M.; Daniels, A. D.; Kudin, K. N.; Strain, M. C.; Farkas, O.; Tomasi, J.; Barone, V.; Cossi, M.; Cammi, R.; Mennucci, B.; Pomelli, C.; Adamo, C.; Clifford, S.; Ochterski, J.; Petersson, G. A.; Ayala, P. Y.; Cui, Q.; Morokuma, K.; Malick, D. K.; Rabuck, A. D.; Raghavachari, K.; Foresman, J. B.; Cioslowski, J.; Ortiz, J. V.; Baboul, A. G.; Stefanov, B. B.; Liu, G.; Liashenko, A.; Piskorz, P.; Komaromi, I.; Gomperts, R.; Martin, R. L.; Fox, D. J.; Keith, T.; Al-Laham, M. A.; Peng, C. Y.; Nanayakkara, A.; Gonzalez, C.; Challacombe, M.; Gill, P. M. W.; Johnson, B.; Chen, W.; Wong, M. W.; Andres, J. L.; Gonzalez, C.; Head-Gordon, M.; Replogle, S.; Pople, J. A. *Gaussian 98*, Revision A.7; Gaussian, Inc.: Pittsburgh, PA, 1998.
(47) Ohmori, N.; Suzuki, T.; Ito, M. *J. Phys. Chem.* **1988**, *92*, 1086−1093.
(48) Ridley, J. E.; Zerner, M. C. *J. Mol. Spectrosc.* **1979**, *76*, 71−85.
(49) Warren, J. A.; Bernstern, E. R. *J. Chem. Phys.* **1986**, *85*, 2365−2367.
(50) Turro, N. J. *Modern Molecular Photochemistry*; University Science Books: 1991.
(51) Bernardi, F.; Olivucci, M.; Robb, M. A. *Chem. Soc. Rev.* **1996**, *25*, 321−328.
(52) Anderson, R. W.; Hochstrasser, R. M.; Lutz, H.; Scott, G. W. *J. Chem. Phys.* **1974**, *61*, 2500−2506.
(53) Morris, J. M.; Williams, D. F. *Chem. Phys. Lett.* **1974**, *25*, 312−314.
(54) Matsumoto, T.; Sato, M.; Hiroyama, S. *Chem. Phys. Lett.* **1972**, *13*, 13−15.
(55) El-Sayed, M. A. *J. Chem. Phys.* **1964**, *41*, 2462−2467.
(56) El-Sayed, M. A.; Leyerle, R. *J. Chem. Phys.* **1975**, *62*, 1579−1580.
(57) Halpern, A.; Ware, W. R. *J. Chem. Phys.* **1970**, *53*, 1969−1977.
(58) Hansen, D. A.; Lee, K. C. *J. Chem. Phys.* **1975**, *62*, 183−189.
(59) Caldwell, R. A.; Fink, P. M. *Tetrahedron Lett.* **1969**, *35*, 2987−2989.
(60) Caldwell, R. A.; Fink, P. M. *Tetrahedron Lett.* **1969**, *47*, 4151−5153.
(61) Harvey, J. N.; Aschi, M. *Phys. Chem. Chem. Phys.* **1999**, *1*, 5555−5563 and references therein.